Tactile-Direction-Sensitive and Stretchable Electronic Skins Based on Human-Skin-Inspired Interlocked Microstructures

Jonghwa Park,[†,#] Youngoh Lee,[†,#] Jaehyung Hong,[‡] Youngsu Lee,[†] Minjeong Ha,[†] Youngdo Jung,[§] Hyuneui Lim,[§] Sung Youb Kim,[‡] and Hyunhyub Ko*[,†]

[†]Department of Energy Engineering, School of Energy and Chemical Engineering, and [‡]School of Mechanical and Nuclear Engineering, Ulsan National Institute of Science and Technology (UNIST), Ulsan Metropolitan City, 689-798, Republic of Korea and [§]Department of Nature-Inspired Nanoconvergence Systems, Korea Institute of Machinery & Materials, Daejeon, 305-343, Republic of Korea. [#]J.-H. Park and Y.-O. Lee contributed equally to this work.

ABSTRACT Stretchable electronic skins with multidirectional force-sensing capabilities are of great importance in robotics, prosthetics, and rehabilitation devices. Inspired by the interlocked microstructures found in epidermal–dermal ridges in human skin, piezoresistive interlocked microdome arrays are employed for stress-direction-sensitive, stretchable electronic skins. Here we show that these arrays possess highly sensitive detection capability of various mechanical stimuli including normal, shear, stretching, bending, and twisting forces. Furthermore, the unique geometry of interlocked microdome arrays enables the differentiation of various mechanical stimuli because the arrays exhibit different levels of deformation depending on the direction of applied forces, thus providing different sensory output patterns. In addition, we show that the electronic skins attached on human skin in the arm and wrist areas are able to distinguish various mechanical stimuli applied in different directions and can selectively monitor different intensities and directions of air flows and vibrations.

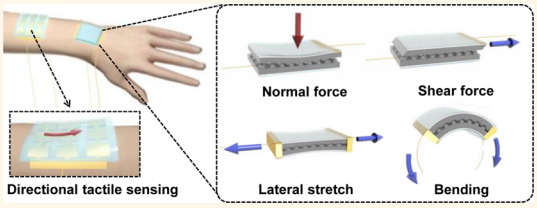

KEYWORDS: stretchable electronic skin · tactile sensor · directional sensor · human-skin-inspired device

Artificial electronic skins that mimic the sensing capabilities of biological skins have recently attracted much attention for a broad range of applications in wearable electronics, prosthetic limbs, robotics, remote surgery, and biomedical devices.[1,2] As an ideal model system for artificial electronic skins, human skin, with various sensory receptors (mechanoreceptor, thermoreceptor, nociceptor, *etc.*), enables the perception of external stimuli such as pressure, shear, strain, vibration, temperature, and pain. In particular, various mechanoreceptors such as the Merkel disk (MD), Meissner corpuscle (MC), Pacinian corpuscle (PC), and Ruffini ending (RE) distributed in the epidermis and dermis layers (see schematic illustration in Figure 1a) provide spatiotemporal recognition of the magnitude, location, and direction of contact forces, which is critically essential when a human manipulates an object.[3] For example, the distribution of normal and shear tangential stresses while making contact with an object provides information on its shape and surface texture, friction between the skin and object, and the accidental slip.[2] The strain pattern on the skin during finger movements is critical to the brain's perception of the position of finger joints relative to the body.[4] In addition to the magnitude of stress, the directional sensitivity to force is critical to maintaining the balance between normal and tangential fingertip forces, which enables the handling of irregular-shaped objects.[5−8]

To fabricate electronic skins that mimic the tactile-sensing capability of human skin, diverse approaches based on various transduction modes, such as those employing resistive,[9−13] capacitive,[14−17] piezoelectric,[18,19] and triboelectric sensors,[20,21] have been suggested. In particular, for the detection of various mechanical and environmental stimuli, multimodal electronic skins have been demonstrated based on the integration of mechanical and physical

* Address correspondence to hyunhko@unist.ac.kr.

Received for review October 18, 2014 and accepted November 12, 2014.

Published online November 12, 2014
10.1021/nn505953t

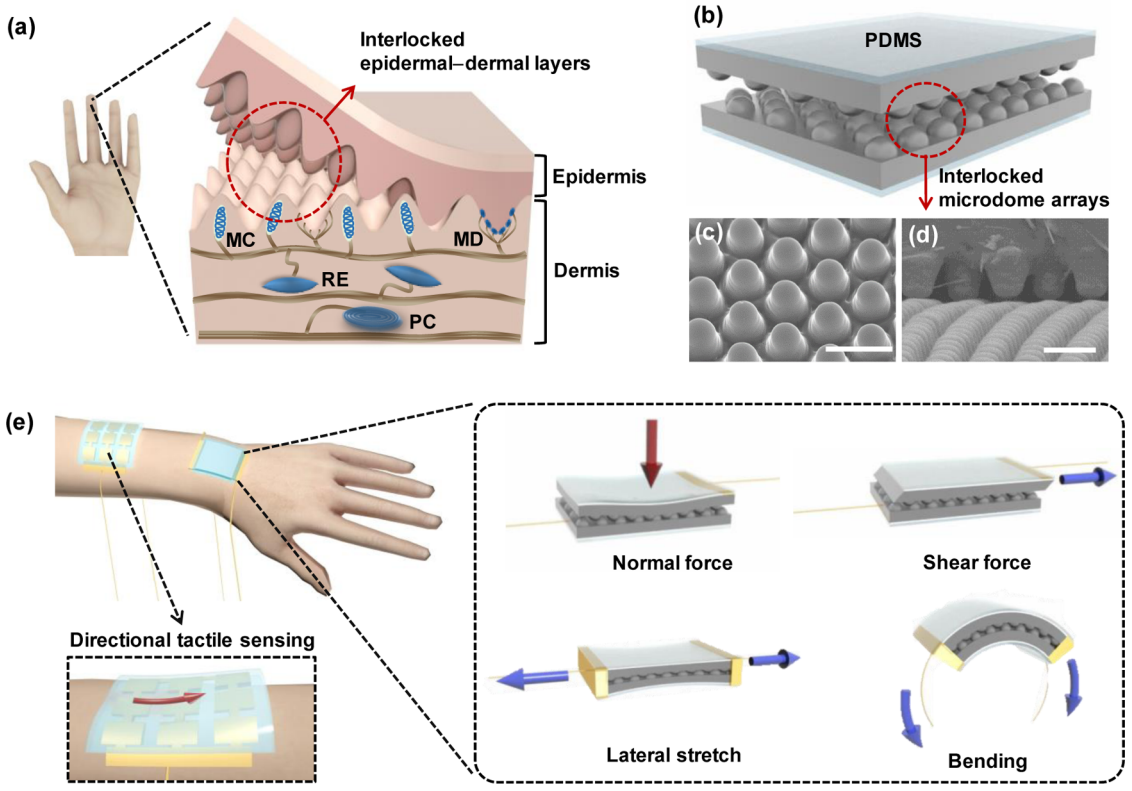

Figure 1. Electronic skin based on carbon nanotube–poly(dimethylsiloxane) (CNT–PDMS) composite films with interlocked microdome arrays. (a) Schematic of human skin structure showing interlocked epidermal–dermal layers and mechanoreceptors (MD: Merkel disk; MC: Meissner corpuscle; PC: Pacinian corpuscle; RE: Ruffini ending). (b) Schematic of an interlocked microdome array. (c) Tilted SEM image of a composite film with microdome arrays (diameter: ~4 μm; height: ~3 μm; pitch: 6 μm). Scale bar: 5 μm. (d) Cross-sectional SEM image of an interlocked composite film. Scale bar: 5 μm. (e) Schematic of a stress-direction-sensitive electronic skin for the detection and differentiation of various mechanical stimuli including normal, shear, stretching, bending, and twisting forces.

sensors on flexible substrates,[22−25] nanostructured conductive composites,[26,27] and organic transistor arrays.[28] However, most of the previous studies either focused on the detection of only one type of mechanical stimuli or developed electronic skins that were not capable of discriminating multiple mechanical stimuli and their directions. There have been several reports on the detection and differentiation of normal and in-plane forces applied to electronic skins.[29−32] Pang *et al.* demonstrated the piezoresistive detection and differentiation of normal, tangential, and torsional forces using Pt-coated micropillar arrays.[31] Gong *et al.* employed tissue papers impregnated with gold nanowires to enable the perception of pressure, bending, torsional forces, and acoustic vibrations.[32] Stretchable electronic skins with multidirectional sensing capabilities have not yet been demonstrated, however. In addition, the low sensitivities of sensors in previous studies provided only small differences in transduced signals under different external forces, which reduced the sensors' capabilities to clearly resolve the intensity and direction of the forces.

In human tactile systems, it has been reported that the intermediate ridges present at the epidermal–dermal junction enhance the tactile perception of mechanoreceptors.[33] Intermediate ridges with the geometry of interlocked microstructures (schematic illustration in Figure 1a) are known to provide strong adhesion between the epidermis and dermis. They also magnify and transduce the tactile stimuli from the skin surface to the mechanoreceptors by concentrating stress near the ridge tips, where mechanoreceptors such as MDs and MCs are located.[2,33,34] Although there are several recent reports on bioinspired adhesion systems[35−37] and electronic skins[31,38] that mimic the interlocked microstructures of beetles and dragonflies, multidirectional, stretchable electronic skins mimicking the interlocked microstructures in human skin have yet to be reported. We have previously reported piezoresistive electronic skins with interlocked microdome arrays for the ultrasensitive detection of normal pressure.[38] In this study, inspired by the interlocked epidermaldermal ridges in human skin, we further explored the interlocked microdome arrays for stress-direction-sensitive and stretchable electronic skins that can detect directional mechanical stimuli applied along three different axes. We fabricated piezoresistive, interlocked microdome arrays in which the interlocked geometry of dome-shaped conductive elastomers enabled stress concentration at the contact

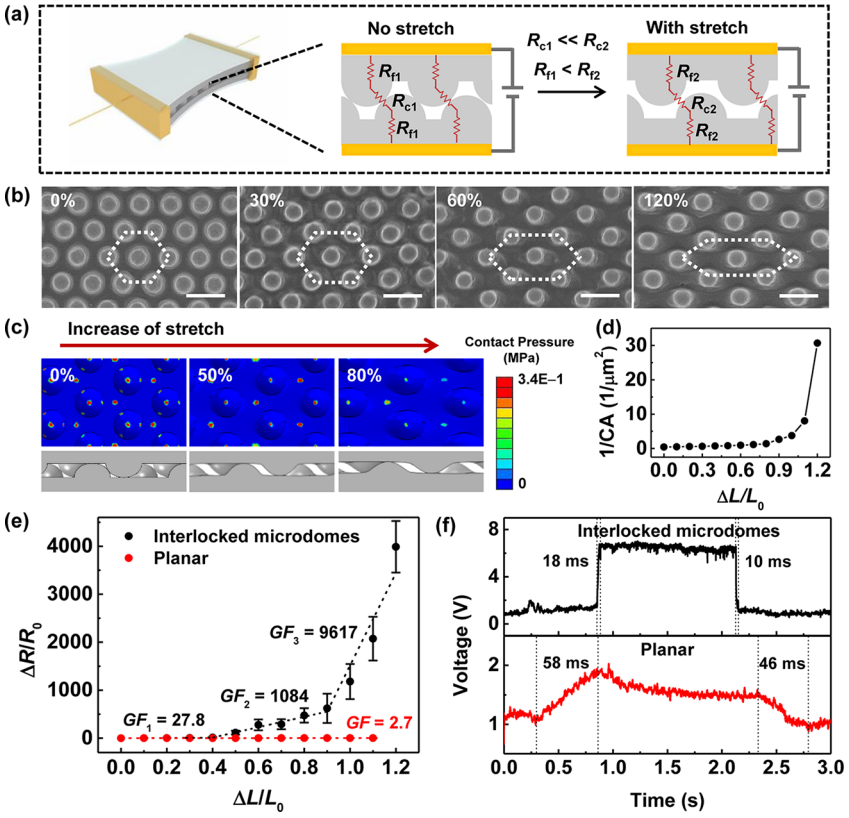

Figure 2. Lateral-stretch-sensing capability of electronic skins. (a) Schematic of the stretch-sensing mechanism of interlocked microdome arrays. (b) SEM images of microdome arrays showing the deformation of the array pattern from hexagons to elongated hexagons under different stretch ratios (0, 30, 60, and 120%). Scale bar: 5 μm. (c) Finite-element analysis showing the contact pressure and the contact points between interlocked microdome arrays with the increase of uniaxial stretch. (d) FEA-calculated results of the change of contact area (CA) between interlocked microdome arrays as a function of stretch. (e) Comparison of stretch-sensing capabilities of interlocked microdome arrays (black) and planar films (red). (f) Comparison of response and relaxation times of interlocked microdome arrays (black) and planar films (red) exposed to a stretching ratio of 50% and stretching speed of 3 mm s^{-1}. The CNT concentration in the composite was 7 wt %, and curing temperature was 60 °C. CNT concentration is 7 wt % for all the results.

points, resulting in the exclusive deformation of microdomes and thus enhanced sensitivity of the piezoresistive response to various tactile stimuli. We also demonstrated that a fully functional wearable electronic skin with 3 × 3 sensor arrays can selectively monitor different intensities and directions of air flow and vibration stimuli.

RESULTS AND DISCUSSION

Bioinspired Interlocked Microdome Arrays. The biomimetic design of the interlocked microdome arrays was based on carbon nanotube (CNT) composite elastomer films with surface microstructures of hexagonal microdome arrays. The interlocked geometry was accomplished by engaging two microdome-patterned CNT composite films with the patterned sides contacting each other. Each elastomeric film with a microdome pattern was fabricated by casting a viscous solution containing multiwalled carbon nanotubes (MWNTs) and poly(dimethylsiloxane) (PDMS) onto a silicon micromold (Figure S1). Figure 1c shows a representative scanning-electron microscope (SEM) image of a microdome-patterned conductive film with microdomes measuring 3 μm in height and 4 μm in diameter and an array pitch of 6 μm. The electronic skin was configured by interlocking two microdome composite films, with the microdomed surfaces facing each other (cross-sectional SEM image in Figure 1d). When the interlocked microdome arrays were attached on human skin in the arm and wrist areas, it was possible to monitor the magnitude and direction of various mechanical stimuli (pressure, shear, strain, and curvature) applied on the electronic skins (Figure 1e).

Stretchable Electronic Skins. The perception of stretch in human skin is critical to the sense of position and movement of fingers, elbows, and knees.[4,39] The stretch-sensing mechanism of the interlocked microdome arrays was based on variations in the contact area between microdomes with changes in the stretch ratio. Figure 2a illustrates the variations in the contact (R_c) and film (R_f) resistances when the interlocked microdome arrays were stretched. The contact resistance (R_c) significantly increased with the decrease in contact area between the microdomes when the gaps between them increased under lateral strain. Compared to the large change in R_c, however, the stretching-induced change in R_f had a minimal effect on the change in overall resistance because the change

of intertube distance within the composite film is small and thus results in the small change of R_f compared to the change of R_c. The small change of R_f is evident from the low gauge factor of planar films in Figure 2e. To elucidate the working principle of the interlocked microdome arrays behind their stretch-sensing capability, we investigated the deformation of the microdome array pattern as a function of lateral strain. As can be seen in the SEM images in Figure 2b, the microdome arrays changed their geometry from hexagons to elongated hexagons in the stretching direction with increasing lateral strain, resulting in the decrease of contact pressure and increases in gap distances between the microdomes. These increased gap distances decreased the contact area between the interlocked microdomes, thus increasing the contact resistance of the interlocked microdome arrays. In order to verify the variations in contact area with the application of lateral strain, we performed finite-element simulations of the change in contact area in the interlocked microdome arrays. Figure 2c shows the changes in contact pressure at various contact points between interlocked microdome arrays with the increase of lateral strain. As the lateral strain increases, both the contact pressure and the number of contact points decrease. Consequently, the decreased contact pressure and the number of contact points results in the decrease of the contact area. The simulation result in Figure 2d shows that the inverse contact area increases exponentially with the increase of lateral strain. Since the inverse contact area is directly proportional to tunneling resistance between contact points,[38] the electrical resistance of interlocked microdome arrays increases exponentially as a function of lateral strain, as can be seen in Figure 2e.

On the basis of a comparison of sensitivity as functions of CNT concentration and curing temperature (Figure S3), we chose a CNT concentration of 7 wt % and a curing temperature of 60 °C as the optimal conditions for the fabrication of stretchable electronic skins. In our previous report, the increase of CNT concentration above the electrical percolation threshold (6 wt %) resulted in the increase of tunnelling piezoresistance of interlocked microdome arrays, but also caused the increase of an elastic modulus of composite films.[38] Therefore, 7 wt % e-skins with higher tunnelling piezoresistance than 6 wt % and larger stretchability than 8 wt % ones result in the highest sensitivity to lateral stretch. E-skins cured at 60 °C showed the highest sensitivity because the decrease of curing temperature leads to the decrease of elastic modulus and thus the increased deformability in response to mechanical stress. Figure 2e shows the change in relative (or normalized) electrical resistance (R/R_0) as a function of applied lateral strain (L/L_0) for the interlocked microdome arrays prepared under these conditions. Here, R_0 and L_0 denote the resistance and length of an electronic skin with and without stretch, respectively. The relative resistance of the interlocked microdome arrays increased significantly with increasing lateral strain, while the planar composite films without interlocked structures showed minimal change in relative electrical resistance. For a quantitative analysis of the strain sensitivity of the electronic skins, the strain gauge factor (GF) is defined as GF = $(R/R_0)/\varepsilon$, where ε is the lateral strain and is defined as $\varepsilon = L/L_0$. The interlocked microdome arrays showed different GF values depending on the lateral strain: 27.8 at a strain of 0−40%, 1084 at a strain of 40−90%, and 9617 at a strain of 90−120%. These GF values are significantly (10−395 times) higher than the values for the planar films (2.7 at a strain of 0−110%), sandwiched Ag-nanowire composites (2−14 at 0−70%),[40] three-dimensional macroporous graphene paper (7.1 at 0−100%),[41] and ZnO−polystyrene nanofiber hybrid films (116 at 0−50%).[42] Although GF values comparable to those of the interlocked microdome arrays have been reported for single-nanotube or single-nanowire sensors (600−1250 at a strain of 0−1.5%)[43,44] and woven graphene films (~10^3 at a strain of 0−6%),[45] their sensing ranges are narrow.

In addition to the high GF values, the interlocked microdome arrays exhibited a narrow hysteresis curve for repeated stretch−release cycles (Figure S2). One of the additional advantages of our electronic skins with interlocked geometry is the fast response time. Generally, the bulk polymer composite films exhibit slow response owing to the viscoelastic behavior of bulk polymers.[46] On the other hand, the interlocked-microdome strain sensor operated mainly through the change in contact area between interlocking microdome arrays, overcoming the viscoelastic delay of bulk polymers. Figure 2f shows the short response (~18 ms) and relaxation (~10 ms) times of the interlocked microdome arrays under repeated strain cycles at 50% lateral strain and a stretching speed of 3 mm s^{-1}, which are 3−4 times faster than those of planar composite films (response and relaxation times of ~58 ms and ~46 ms, respectively). The arrays' response and relaxation times are comparable to those of ZnO-nanowire piezotronic strain sensors (~10 ms)[43] and much shorter than values obtained for Sb-doped ZnO nanobelt sensors (0.6−3 s)[47] and CNT−silver nanoparticle composite sensors (~100 ms).[48]

Shear-Force Sensitivity. In addition to their stretch-sensing capability with high GF values, the capability of electronic skins to detect and differentiate normal and shear forces is critical in the perception of slip motion, force direction, and strength, as well as the dexterous manipulation of objects for applications in bionic hands, grippers, and tactile displays.[49−52] Our sensor is ideal for the detection of shear stress because the interlocked geometry of microdome arrays provides a strong joint without slip and thus enables the concentration of shear stress at the contact

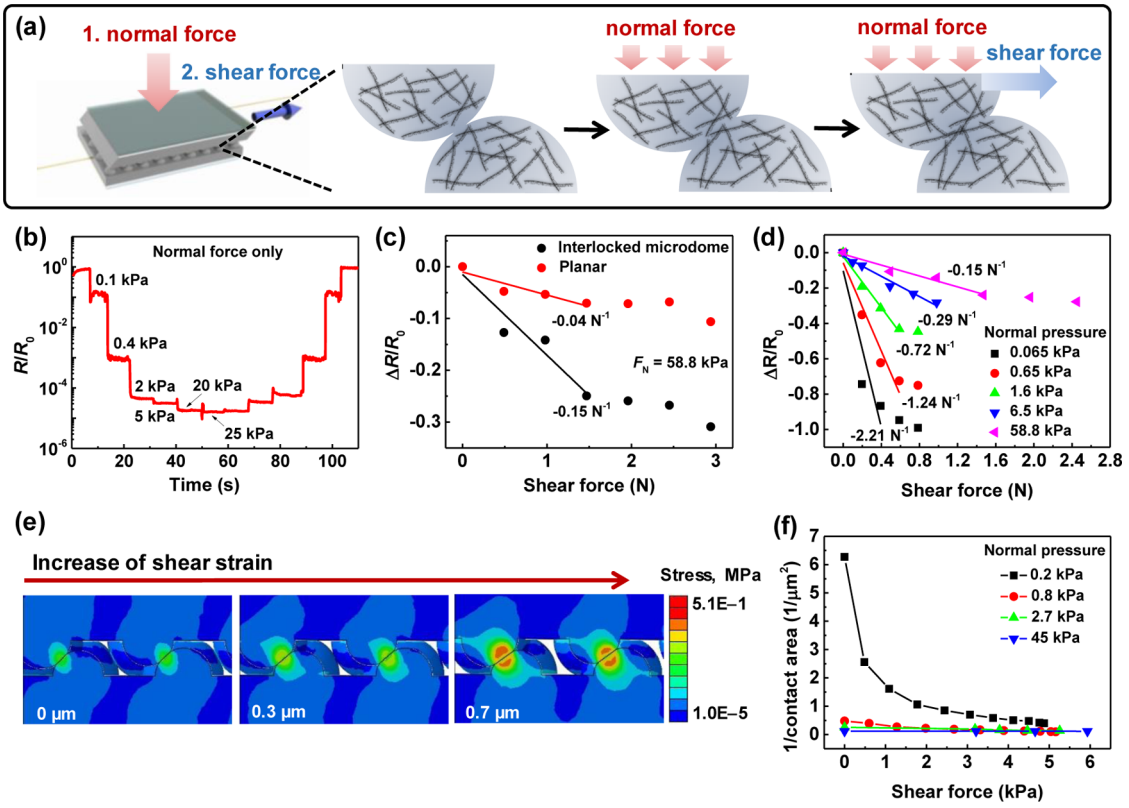

Figure 3. Normal- and shear-force-sensing capabilities of electronic skins. (a) Schematic of the deformation of interlocked microdomes during successive applications of normal and shear forces. (b) Relative electrical resistance of electronic skin sample as a function of normal force. (c) Comparison of shear-force sensitivities of interlocked microdomes (black) and planar (red) films under a normal pressure of 58.8 kPa. (d) Comparison of shear-force sensitivities of interlocked microdome arrays under different normal pressures. (e) Finite-element analysis (FEA) showing the deformation and local stress distribution of interlocked microdome arrays with increasing shear force at a normal pressure of 45 kPa. (f) Calculated FEA results of the inverse contact area as a function of shear force under different normal pressures. The CNT concentration was 7 wt % in all electronic skins used for the measurements.

spots. In addition, in our system, the changes in contact resistance were different in response to the normal and shear forces, leading to the differentiation between normal and shear stresses. To test the normal- and shear-force sensitivity, the samples were preloaded with a normal pressure to engage the upper and lower microdome arrays and subsequently subjected to a known value of shear force (Figure 3a). The applied normal force immediately induced the surface deformation of microdomes in the interlocked geometry, resulting in an increase in contact area and thus a decrease in contact resistance between the interlocked microdomes. Figure 3b shows that the interlocked microdome arrays exhibited a systematic and consistent decrease and increase in relative resistance when the applied normal pressure was reversibly varied from 100 Pa to 25 kPa. As demonstrated in our previous study,[38] the high sensitivity to the normal force can be attributed to the significant change in tunnelling piezoresistance at the contact spots between the interlocked microdome arrays.

The subsequent application of a shear force resulted in the microdome deformation in the lateral direction, which led to a further increase in contact area between the microdomes and a decrease in contact resistance. Figure 3c shows the change in relative resistance of interlocked microdome arrays as a function of shear force under a normal force (F_N) of 58.8 kPa. For the quantitative analysis, we define a shear-force sensitivity (S) in the linear range for different normal pressure loadings as $S = (\Delta R/R_0)/(\Delta F_S)$), where R and F_S are the resistance and applied shear force, respectively. The interlocked microdome arrays exhibited a shear-force sensitivity of 0.15 N^{-1}, which is approximately 4 times the sensitivity of a planar film. Because the normal pressure affected the initial contact area between the interlocked microdome arrays, the shear-force sensitivity could be manipulated by controlling the normal pressure to engage the microdome arrays. Figure 3d shows the change in relative resistance as a function of shear force for different loadings of normal pressure for electronic skins with 7 wt % CNTs. We observed that the shear-force sensitivity increased with a decrease in normal pressure. The largest sensitivity was 2.21 N^{-1} for a normal pressure of 65 Pa, which is ~13 times the sensitivity (0.15 N^{-1}) at a normal pressure of 58.8 kPa. This behavior can be explained by the decreased initial contact area between microdome arrays at a lower normal pressure, providing the possibility to further increase the contact area by applying a shear force. Figure S4 shows the

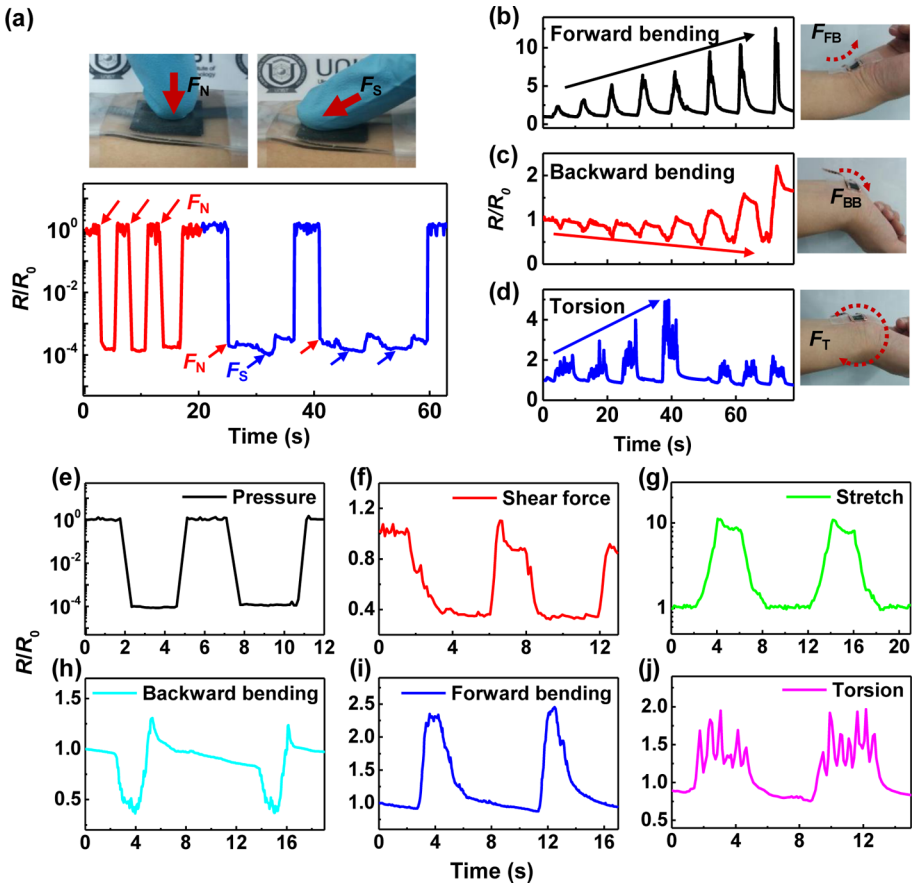

Figure 4. Stress-direction-sensitive electronic skins for the detection and differentiation of multiple mechanical stimuli. (a) Real-time monitoring of changes in the relative resistance of interlocked microdome arrays subjected to different normal and shear forces. (b–d) Change in relative electrical resistance of an electronic skin attached on the front of a human wrist under different types of wrist movements: (b) forward bending; (c) backward bending; (d) torsion. The electronic skin showed different signal patterns in response to different wrist movements. (e–j) Change in relative electrical resistance of electronic skins in response to different mechanical stimuli: (e) normal force; (f) shear force; (g) lateral stretch; (h) forward bending; (i) backward bending; (j) torsion.

decrease and increase in the relative resistance of interlocked microdome arrays during pulling and retracting cycles under different shear forces, which also demonstrate their reliability.

In order to verify the variations in contact area with the application of normal and shear forces, we performed finite-element simulations of the change in contact area in the interlocked microdome arrays. The simulation results in Figure 3e indicate that the unique structure of interlocked microdome arrays leads to stress concentration and thus deformation of microdomes at the contact spots between spherical microdomes under normal pressure. The subsequent application of shear strain induces further deformation of microdomes at the contact spots, resulting in an increase in contact area. The contact area gradually increases with further increase in shear force, but more importantly, this increase in contact area depends on the normal pressure loadings. As can be seen in Figure 3f, the change in the inverse contact area as a function of shear force is greatest for a normal pressure of 0.2 kPa. At higher values of normal pressure, the variation in inverse contact area decreases with increasing shear force. In addition to the normal force, our experiments showed that the shear-force sensitivity could be further manipulated by controlling the CNT concentration. As shown in Figure S5, the shear-force sensitivity increased with decreasing CNT concentration, with a sensitivity of 0.44 N^{-1} for 5 wt % CNTs, which is ~3 times the sensitivity of the sensor with 7 wt % CNTs (0.15 N^{-1}) at a normal pressure of 58.8 kPa.

Differentiation of Multiple Mechanical Stimuli. Since the interlocked geometry of the microdome arrays provided different deformation patterns specific to the type of mechanical stress, the interlocked microdome arrays were able to detect and differentiate multiple mechanical stimuli. To test their skin-like sensing capabilities, we monitored the normal and shear forces through simple finger contact on the electronic skins attached on human skin. Figure 4a shows the change in relative electrical resistance with repeated application of normal forces of l kPa and then shear forces. The electronic skin showed different signal intensities and patterns for different types of mechanical stimulus. While a finger touching the electronic skin in the normal direction (F_N) resulted in an immediate decrease in

relative resistance, a finger touching the electronic skin in the shear direction, which contained both normal and shear forces ($F_N + F_S$), resulted in additional decreases in the relative electrical resistance. It is worth noting that the patterns of decrease in relative resistance resulting from F_N and F_S were different, therefore allowing the differentiation between normal and shear forces.

Figure 4b–d show that the electronic skin attached on the front of a human wrist could detect and differentiate different types of wrist movements such as forward bending (F_{FB}), backward bending (F_{BB}), and torsion (F_T). In this experiment, we utilized a curing temperature of 60 °C since we observed that a lower curing temperature resulted in higher bending sensitivity (Figure S6). When the electronic skin was bent forward (F_{FB}), the relative electrical resistance increased (Figure 4b); a gradual increase in forward bending resulted in the gradual increase in relative resistance. On the other hand, the relative electrical resistance decreased under backward bending (Figure 4c), while the twisting of the wrist (F_T) resulted in an increase in electrical resistance. In particular, twisting also generated oscillating signals resulting from the repeated contact-on/contact-off behavior during the twisting. These different signal patterns in response to different mechanical stimuli are attributed to the unique interlocked geometry of microdome arrays, which, depending on the direction of mechanical stress, could result in distinct variations in contact area. During forward bending, the gap between the neighboring microdome arrays increased because the upper microdome layer tends to detach from the lower microdome layer due to the strain mismatch between the upper (under tension) and lower (under compression) microdome arrays, leading to an increase in relative resistance. Backward bending decreased the electrical resistance because the lower microdome layer is sandwiched between the human skin and the upper microdome layer, resulting in the decreased gaps between adjacent microdome arrays.

Figure 4e–j show that the different deformation patterns of interlocked microdome arrays depending on the type of mechanical stress result in the differentiation of multiple mechanical stimuli. Here, each of the electrical signals under different mechanical stimuli provides a unique output pattern specific to the type of mechanical input, leading to the differentiation of multiple mechanical stimuli. This capability is facilitated by the tactile-direction-sensitive deformation of interlocked microdome arrays, which results in the different magnitudes of deformations and response/relaxation times. As can be seen in Figure 4e–j, the relative resistances decrease for pressure, shear, and backward bending forces and increase for stretch, forward bending, and torsional forces. In particular, the pattern of resistance variation can be differentiated by the different magnitude, shape, and response/relaxation times. In addition, the torsional force generates unique oscillation patterns in the resistance variation, which can be attributed to the repeated contact area variation during the continuous twisting of regular microdome arrays. Although the basic principle of differentiating various tactile stimuli in our e-skin is different from that of human skin with various mechanoreceptors, the results in this study also suggest that the interlocked microstructures of human skin may have profound effects on the differentiation of various tactile signals. In the future, mimicking the mechanoreceptors in epidermis and dermis layers of human skin in addition to the interlocked microstructures may enable e-skins with realistic human-skin-like tactile sensing capabilities.

Wearable Electronic Skins with Stress-Direction Sensitivity. For the proof-of-concept wearable electronic skins to resolve the spatial distribution and the directions of applied external stimuli such as touch, flow, and vibration, we fabricated 3 × 3 pixel arrays of electronic skin sandwiched between cross arrays of platinum electrodes (Figure 5a). When we touched two different pixels (R1-C3 and R3-C1 in Figure 5b) on the electronic skin, it could provide spatially resolved mapping of the touch positions. The high sensitivity of each pixel on the electronic skin could also provide the ability to resolve gradual changes in mechanical stimuli, therefore enabling the detection of the direction of mechanical stress. Figure 5c shows that depending on the finger-pushing directions (left, right, up, and down), the electronic skin exhibited different spatially resolvable patterns, indicating the perception of the intensity and direction of tactile stimuli. Figure 5d also demonstrates the directional sensing capability of the electronic skin, where fluid flows in different directions (left, right, and diagonal) could be clearly resolved by the signal patterns. The sensitivity to gradual changes and directions of external stimuli was also verified by applying a vibrational stimulus on the electronic skin. Figure 5e shows the application of radial vibration on one pixel located at the corner (R1-C1) of the electronic skin and the resulting spatial mapping of the vibrational stimulus. Owing to vibrational damping, the change in relative resistance gradually decreased as the pixel location was farther away from the original pixel at which vibration was applied, which led to gradually decreasing changes in the relative resistance.

CONCLUSIONS

In summary, we have demonstrated stress-direction-sensitive and stretchable electronic skins with three-axial stress-sensing capabilities. We employed piezoresistive, interlocked microdome arrays that were inspired by the interlocked epidermal–dermal layers in human skin. Similar to the stress-concentrating function of interlocked epidermal–dermal ridges, which magnify the tactile stimuli, the arrays could induce exclusive stress concentration at the contact spot and

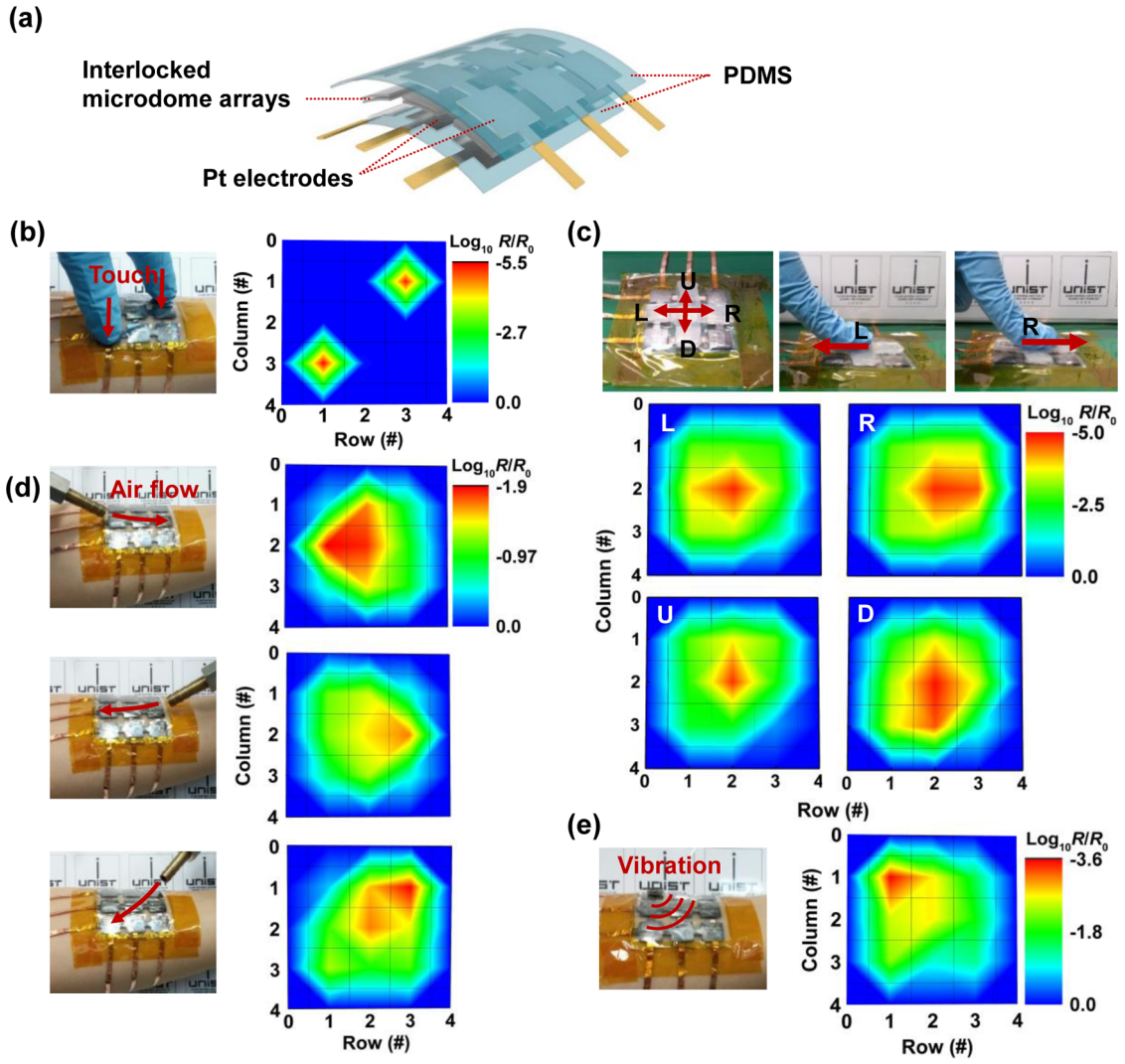

Figure 5. Stress-direction-sensitive electronic skins for directional sensing of mechanical stimuli applied in three axial directions. (a) Schematic of sensor arrays, where interlocked microdome arrays are sandwiched between the electrodes and PDMS protection layers. (b) Spatial pressure mapping capability of electronic skin for the detection of finger touch on two different pixels (R1-C3, R3-C1). (c) Detection of different finger-pushing directions: left (L), right (R), up (U), down (D). (d) Detection of different directions of fluid flow (left, right, diagonal). (e) Detection of the location of applied vibration and the gradual damping of vibration.

thus deformation of the microdomes, resulting in enhanced sensitivity of the piezoresistive response to stress. In particular, the unique geometry of the interlocked microdome arrays led to different deformation patterns that depend on the type and direction of mechanical stress, enabling detection and differentiation of various mechanical stimuli including normal, shear, stretch, bending, and twisting forces. Owing to the direction-sensitive tactile-sensing properties, various electronic skins attached on human skin were successfully employed to monitor different intensities and directions of finger touches, air flows, and vibrations. Because our design is the simplified version of complicated human skin, where papillary ridges, location of mechanoreceptors, the elastic moduli of layers, and the shape and size of intermediate ridges are all closely related to each other to efficiently transduce and magnify tactile stimuli, we expect that the interlocked geometry can be further explored to develop bioinspired electronic skins with human-skin-like tactile-sensing capabilities. Finally, we anticipate that our stretchable electronic skins with multidirectional stress-sensing capabilities can find applications in robotic skins, prosthetic limbs, and rehabilitation devices to monitor motion and stress distribution.

EXPERIMENTAL SECTION

Fabrication of Elastic Composite Film with Microdome Arrays. For the fabrication of composite elastomers, MWNTs (Sigma-Aldrich) with diameters of 110−190 nm and lengths of 5−9 μm were first dispersed in chloroform by sonication for 6 h. Using a vortex mixer, the dispersed solution was mixed with a PDMS base (Sylgard 184, Dow Corning) at different ratios (5−8 wt %) of

MWNTs to PDMS, followed by heating at 90 °C on a hot plate to remove the chloroform. For the micromolding process, hexane and a PDMS curing agent (1:10 ratio for the curing agent and PDMS base) were added to each MWNT–PDMS composite mixture (concentration of 500 mg mL^{-1}) and then mixed with a vortex mixer for 5 min. These composite mixtures were cast onto silicon micromolds with hexagonal hole arrays (diameter: 3.5 μm, pitch size: 6 μm) and stored in a vacuum desiccator for 1 h to remove the residual hexane. Finally, different microdome-patterned MWNT–PDMS composite films (thickness of 500 μm) were prepared by thermal curing at 60–80 °C (strain and curvature sensors: 60 °C, pressure and shear-force sensors: 70 °C) for 3 h. For the electronic-skin applications, the interlocked microdome-patterned films were coated with platinum on both sides by a sputter coating system (K575X, Quorum Emitech) to form electrode arrays. To minimize the contact resistance, a silver paste was applied between the composite film and Pt electrode and annealed at 100 °C for 1 h.

Characterization. The surface morphologies of the microdome composite films were characterized by a field-emission SEM (FE-SEM; S-4800, Hitachi) and an optical microscope (PSM-1000, Olympus). The piezoresistive properties of the electronic skins were measured using a two-probe method (4200-SCS, Keithley) at 10 V. To apply mechanical forces on the electronic skins, a pushing tester (JIPT-100, Junil Tech) was used to provide normal forces, and a tensile/bending machine (JIBT-200, Junil Tech) was used to provide lateral and bending strain. For the tangential-shear tactile-sensing measurements, a polyethylene terephthalate (PET) film was attached on one side of a composite film, and one end of the PET film was connected to a force gauge in the tangential direction. A constant normal force was then applied on the electronic skin using a lab-built microstage system (Micro Motion Technology, Korea), after which a shear force was applied to the electronic skin. For the evaluation of the directional tactile-sensing properties, a flow meter (Ar gas, flow rate of 5.3 m s^{-1}) and a vibrator (2.0 m s^{-2}) were used to provide mechanical stimuli in different directions.

Finite-Element Method. For the contact area calculations under stretching and shearing, we conducted structural analyses using the finite-element method. Composite films with interlocked microdomes arrays were modeled as linear elastic materials described by experimentally measured elastic constants.[38] We employed more than 2.8 million four-node linear tetragonal elements with adaptive mesh-refinement scheme around the contact area. All calculations were static under proper loading conditions, and the mechanical contact between two deformable surfaces was calculated by a surface-to-surface contact scheme.

Conflict of Interest: The authors declare no competing financial interest.

Supporting Information Available: Microdome array fabrication, hysteresis, and reliability of piezoresistivities, temperature, and CNT concentration dependent stretch and bending tests, and shear-force sensitivity as a function of CNT concentration. This material is available free of charge *via* the Internet at http://pubs.acs.org.

Acknowledgment. This work was supported by the National Research Foundation of Korea (NRF-2011-0014965, NRF-2012K1A3A1A20031618) and Korea Institute of Machinery & Materials (KIMM) (NK175B).

REFERENCES AND NOTES

1. Hammock, M. L.; Chortos, A.; Tee, B. C. K.; Tok, J. B. H.; Bao, Z. 25th Anniversary Article: The Evolution of Electronic Skin (E-Skin): A Brief History, Design Considerations, and Recent Progress. *Adv. Mater.* **2013**, *25*, 5997–6038.
2. Dahiya, R. S.; Metta, G.; Valle, M.; Sandini, G. Tactile Sensing—from Humans to Humanoids. *Robotics, IEEE Trans. Robotics* **2010**, *26*, 1–20.
3. Delmas, P.; Hao, J. Z.; Rodat-Despoix, L.; Rodat-Despoix, L. Molecular Mechanisms of Mechanotransduction in Mammalian Sensory Neurons. *Nat. Rev. Neurosci.* **2011**, *12*, 139–153.
4. Edin, B. B.; Johansson, N. Skin Strain Patterns Provide Kinaesthetic Information to the Human Central Nervous System. *J. Physiol.* **1995**, *487*, 243–251.
5. Birznieks, I.; Jenmalm, P.; Goodwin, A. W.; Johansson, R. S. Encoding of Direction of Fingertip Forces by Human Tactile Afferents. *J. Neurosci.* **2001**, *21*, 8222–8237.
6. Dobrzynska, J. A.; Gijs, M. Polymer-Based Flexible Capacitive Sensor for Three-Axial Force Measurements. *J. Micromech. Microeng.* **2013**, *23*, 015009.
7. Lee, H.-K.; Chung, J.; Chang, S.-I.; Yoon, E. Real-Time Measurement of the Three-Axis Contact Force Distribution Using a Flexible Capacitive Polymer Tactile Sensor. *J. Micromech. Microeng.* **2011**, *21*, 035010.
8. Surapaneni, R.; Guo, Q.; Xie, Y.; Young, D. J.; Mastrangelo, C. H. A Three-Axis High-Resolution Capacitive Tactile Imager System Based on Floating Comb Electrodes. *J. Micromech. Microeng.* **2013**, *23*, 075004.
9. Sekitani, T.; Yokota, T.; Zschieschang, U.; Klauk, H.; Bauer, S.; Takeuchi, K.; Takamiya, M.; Sakurai, T.; Someya, T. Organic Nonvolatile Memory Transistors for Flexible Sensor Arrays. *Science* **2009**, *326*, 1516–1519.
10. Takei, K.; Takahashi, T.; Ho, J. C.; Ko, H.; Gillies, A. G.; Leu, P. W.; Fearing, R. S.; Javey, A. Nanowire Active-Matrix Circuitry for Low-Voltage Macroscale Artificial Skin. *Nat. Mater.* **2010**, *9*, 821–826.
11. Yamada, T.; Hayamizu, Y.; Yamamoto, Y.; Yomogida, Y.; Izadi-Najafabadi, A.; Futaba, D. N.; Hata, K. A Stretchable Carbon Nanotube Strain Sensor for Human-Motion Detection. *Nat. Nanotechnol.* **2011**, *6*, 296–301.
12. Tee, B. C.; Wang, C.; Allen, R.; Bao, Z. An Electrically and Mechanically Self-Healing Composite with Pressure-and Flexion-Sensitive Properties for Electronic Skin Applications. *Nat. Nanotechnol.* **2012**, *7*, 825–832.
13. Wang, C.; Hwang, D.; Yu, Z.; Takei, K.; Park, J.; Chen, T.; Ma, B.; Javey, A. User-Interactive Electronic Skin for Instantaneous Pressure Visualization. *Nat. Mater.* **2013**, *12*, 899–904.
14. Cohen, D. J.; Mitra, D.; Peterson, K.; Maharbiz, M. M. A Highly Elastic, Capacitive Strain Gauge Based on Percolating Nanotube Networks. *Nano Lett.* **2012**, *12*, 1821–1825.
15. Mannsfeld, S. C.; Tee, B. C.; Stoltenberg, R. M.; Chen, C. V. H.; Barman, S.; Muir, B. V.; Sokolov, A. N.; Reese, C.; Bao, Z. Highly Sensitive Flexible Pressure Sensors with Microstructured Rubber Dielectric Layers. *Nat. Mater.* **2010**, *9*, 859–864.
16. Lipomi, D. J.; Vosgueritchian, M.; Tee, B. C.; Hellstrom, S. L.; Lee, J. A.; Fox, C. H.; Bao, Z. Skin-Like Pressure and Strain Sensors Based on Transparent Elastic Films of Carbon Nanotubes. *Nat. Nanotechnol.* **2011**, *6*, 788–792.
17. Schwartz, G.; Tee, B. C.-K.; Mei, J.; Appleton, A. L.; Kim, D. H.; Wang, H.; Bao, Z. Flexible Polymer Transistors with High Pressure Sensitivity for Application in Electronic Skin and Health Monitoring. *Nat. Commun.* **2013**, *4*, 1859–1866.
18. Persano, L.; Dagdeviren, C.; Su, Y.; Zhang, Y.; Girardo, S.; Pisignano, D.; Huang, Y.; Rogers, J. A. High Performance Piezoelectric Devices Based on Aligned Arrays of Nanofibers of Poly (vinylidenefluoride-co-trifluoroethylene). *Nat. Commun.* **2013**, *4*, 1633–1642.
19. Wu, W.; Wen, X.; Wang, Z. L. Taxel-Addressable Matrix of Vertical-Nanowire Piezotronic Transistors for Active and Adaptive Tactile Imaging. *Science* **2013**, *340*, 952–957.
20. Fan, F.-R.; Lin, L.; Zhu, G.; Wu, W.; Zhang, R.; Wang, Z. L. Transparent Triboelectric Nanogenerators and Self-Powered Pressure Sensors Based on Micropatterned Plastic Films. *Nano Lett.* **2012**, *12*, 3109–3114.
21. Zhang, X.-S.; Han, M.-D.; Wang, R.-X.; Zhu, F.-Y.; Li, Z.-H.; Wang, W.; Zhang, H.-X. Frequency-Multiplication High-Output Triboelectric Nanogenerator for Sustainably Powering Biomedical Microsystems. *Nano Lett.* **2013**, *13*, 1168–1172.
22. Yeo, W. H.; Kim, Y. S.; Lee, J.; Ameen, A.; Shi, L.; Li, M.; Wang, S.; Ma, R.; Jin, S. H.; Kang, Z.; Huang, Y.; Rogers, J. A. Multifunctional Epidermal Electronics Printed Directly onto the Skin. *Adv. Mater.* **2013**, *25*, 2773–2778.
23. Son, D.; Lee, J.; Qiao, S.; Ghaffari, R.; Kim, J.; Lee, J. E.; Song, C.; Kim, S. J.; Lee, D. J.; Jun, S. W.; Yang, S.; Park, M.; Shin, J.;

Do, K.; Lee, M.; Kang, K.; Hwang, C. S.; Lu, N.; Hyeon, T.; Kim, D. H. Multifunctional Wearable Devices for Diagnosis and Therapy of Movement Disorders. *Nat. Nanotechnol.* **2014**, *9*, 397–404.
24. Xu, L.; Gutbrod, S. R.; Bonifas, A. P.; Su, Y.; Sulkin, M. S.; Lu, N.; Chung, H. J.; Jang, K. I.; Liu, Z.; Ying, M.; Lu, C.; Webb, R. C.; Kim, J. S.; Laughner, J. I.; Cheng, H.; Liu, Y.; Ameen, A.; Jeong, J. W.; Kim, G. T.; Huang, Y.; Efimov, I. R.; Rogers, J. A. 3D Multifunctional Integumentary Membranes for Spatiotemporal Cardiac Measurements and Stimulation across the Entire Epicardium. *Nat. Commun.* **2014**, *5*, 3329–3338.
25. Kim, D. H.; Lu, N.; Ghaffari, R.; Kim, Y. S.; Lee, S. P.; Xu, L.; Wu, J.; Kim, R. H.; Song, J.; Liu, Z.; Viventi, J.; de Graff, B.; Elolampi, B.; Mansour, M.; Slepian, M. J.; Hwang, S.; Moss, J. D.; Won, S. M.; Huang, Y.; Litt, B.; Rogers, J. A. Materials for Multifunctional Balloon Catheters with Capabilities in Cardiac Electrophysiological Mapping and Ablation Therapy. *Nat. Mater.* **2011**, *10*, 316–323.
26. Harada, S.; Honda, W.; Arie, T.; Akita, S.; Takei, K. Fully Printed, Highly Sensitive Multifunctional Artificial Electronic Whisker Arrays Integrated with Strain and Temperature Sensors. *ACS Nano* **2014**, *8*, 3921–3927.
27. Hou, C.; Wang, H.; Zhang, Q.; Li, Y.; Zhu, M. Highly Conductive, Flexible, and Compressible All-Graphene Passive Electronic Skin for Sensing Human Touch. *Adv. Mater.* **2014**, *26*, 5018–5024.
28. Tien, N. T.; Jeon, S.; Kim, D. I.; Trung, T. Q.; Jang, M.; Hwang, B. U.; Byun, K. E.; Bae, J.; Lee, E.; Tok, J. B.; Bao, Z.; Lee, N. E.; Park, J. J. A Flexible Bimodal Sensor Array for Simultaneous Sensing of Pressure and Temperature. *Adv. Mater.* **2014**, *26*, 796–804.
29. Vogt, D. M.; Park, Y. L.; Wood, R. J. Design and Characterization of a Soft Multi-Axis Force Sensor Using Embedded Microfluidic Channels. *IEEE Sens. J.* **2013**, *13*, 4056–4064.
30. Viry, L.; Levi, A.; Totaro, M.; Mondini, A.; Mattoli, V.; Mazzolai, B.; Beccai, L. Flexible Three-Axial Force Sensor for Soft and Highly Sensitive Artificial Touch. *Adv. Mater.* **2014**, *26*, 2659–2664.
31. Pang, C.; Lee, G.-Y.; Kim, T.-i.; Kim, S. M.; Kim, H. N.; Ahn, S.-H.; Suh, K.-Y. A Flexible and Highly Sensitive Strain-Gauge Sensor Using Reversible Interlocking of Nanofibres. *Nat. Mater.* **2012**, *11*, 795–801.
32. Gong, S.; Schwalb, W.; Wang, Y.; Chen, Y.; Tang, Y.; Si, J.; Shirinzadeh, B.; Cheng, W. A Wearable and Highly Sensitive Pressure Sensor with Ultrathin Gold Nanowires. *Nat. Commun.* **2014**, *5*, 3132–3139.
33. Cauna, N. Nature and Functions of the Papillary Ridges of the Digital Skin. *Anat. Rec.* **1954**, *119*, 449–468.
34. Gerling, G. J.; Thomas, G. W. The Effect of Fingertip Microstructures on Tactile Edge Perception. *Proceedings of the First Joint Eurohaptics Conference and Symposium on Haptic Interfaces for Virtual Environment Teleoperator Systems*; IEEE Computer Society: Washington, D.C., USA, 2005; pp 63−72.
35. Ko, H.; Lee, J.; Schubert, B. E.; Chueh, Y. L.; Leu, P. W.; Fearing, R. S.; Javey, A. Hybrid Core-Shell Nanowire Forests as Self-Selective Chemical Connectors. *Nano Lett.* **2009**, *9*, 2054–2058.
36. Ko, H.; Zhang, Z. X.; Chueh, Y. L.; Ho, J. C.; Lee, J.; Fearing, R. S.; Javey, A. Wet and Dry Adhesion Properties of Self-Selective Nanowire Connectors. *Adv. Funct. Mater.* **2009**, *19*, 3098–3102.
37. Pang, C.; Kim, T. I.; Bae, W. G.; Kang, D.; Kim, S. M.; Suh, K. Y. Bioinspired Reversible Interlocker Using Regularly Arrayed High Aspect-Ratio Polymer Fibers. *Adv. Mater.* **2012**, *24*, 475–479.
38. Park, J.; Lee, Y.; Hong, J.; Ha, M.; Jung, Y. D.; Lim, H.; Kim, S. Y.; Ko, H. Giant Tunneling Piezoresistance of Composite Elastomers with Interlocked Microdome Arrays for Ultrasensitive and Multimodal Electronic Skins. *ACS Nano* **2014**, *8*, 4689–4697.
39. Collins, D. F.; Refshauge, K. M.; Todd, G.; Gandevia, S. C. Cutaneous Receptors Contribute to Kinesthesia at the Index Finger, Elbow, and Knee. *J. Neurophysiol.* **2005**, *94*, 1699–1706.
40. Amjadi, M.; Pichitpajongkit, A.; Lee, S.; Ryu, S.; Park, I. Highly Stretchable and Sensitive Strain Sensor Based on Silver Nanowire-Elastomer Nanocomposite. *ACS Nano* **2014**, *8*, 5154–5163.
41. Yan, C.; Wang, J.; Kang, W.; Cui, M.; Wang, X.; Foo, C. Y.; Chee, K. J.; Lee, P. S. Highly Stretchable Piezoresistive Graphene-Nanocellulose Nanopaper for Strain Sensors. *Adv. Mater.* **2014**, *26*, 2022–2027.
42. Xiao, X.; Yuan, L.; Zhong, J.; Ding, T.; Liu, Y.; Cai, Z.; Rong, Y.; Han, H.; Zhou, J.; Wang, Z. L. High-Strain Sensors Based on ZnO Nanowire/Polystyrene Hybridized Flexible Films. *Adv. Mater.* **2011**, *23*, 5440–5444.
43. Zhou, J.; Gu, Y.; Fei, P.; Mai, W.; Gao, Y.; Yang, R.; Bao, G.; Wang, Z. L. Flexible Piezotronic Strain Sensor. *Nano Lett.* **2008**, *8*, 3035–3040.
44. Cao, J.; Wang, Q.; Dai, H. Electromechanical Properties of Metallic, Quasimetallic, and Semiconducting Carbon Nanotubes under Stretching. *Phys. Rev. Lett.* **2003**, *90*, 157601.
45. Li, X.; Zhang, R.; Yu, W.; Wang, K.; Wei, J.; Wu, D.; Cao, A.; Li, Z.; Cheng, Y.; Zheng, Q. Stretchable and Highly Sensitive Graphene-on-Polymer Strain Sensors. *Sci. Rep.* **2012**, *2*, 870–875.
46. Liu, C.-X.; Choi, J.-W. Strain-Dependent Resistance of PDMS and Carbon Nanotubes Composite Microstructures. *IEEE Trans. Nanotechnol.* **2010**, *9*, 590–595.
47. Yang, Y.; Guo, W.; Qi, J.; Zhang, Y. Flexible Piezoresistive Strain Sensor Based on Single Sb-Doped ZnO Nanobelts. *Appl. Phys. Lett.* **2010**, *97*, 223107.
48. Takei, K.; Yu, Z.; Zheng, M.; Ota, H.; Takahashi, T.; Javey, A. Highly Sensitive Electronic Whiskers Based on Patterned Carbon Nanotube and Silver Nanoparticle Composite Films. *Proc. Natl. Acad. Sci. U.S.A.* **2014**, *111*, 1703–1707.
49. Lee, H. K.; Chung, J.; Chang, S. I.; Yoon, E. Normal and Shear Force Measurement Using a Flexible Polymer Tactile Sensor with Embedded Multiple Capacitors. *J. Microelectromech. Syst.* **2008**, *17*, 934–942.
50. Teshigawara, S.; Shimizu, S.; Tadakuma, K.; Aiguo, M.; Shimojo, M.; Ishikawa, M. High Sensitivity Slip Sensor Using Pressure Conductive Rubber. *IEEE Sensors 2009 Conf.* **2009**, 988–991.
51. Vatani, M.; Engeberg, E. D.; Choi, J. W. Force and Slip Detection with Direct-Write Compliant Tactile Sensors Using Multi-Walled Carbon Nanotube/Polymer Composites. *Sens. Actuator A: Phys.* **2013**, *195*, 90–97.
52. Gleeson, B. T.; Horschel, S. K.; Provancher, W. R. Design of a Fingertip-Mounted Tactile Display with Tangential Skin Displacement Feedback. *IEEE Trans. Haptics* **2010**, *3*, 297–301.